Viologen as an electrolyte additive for extreme fast charging of lithium-ion batteries

Battery Energy

WILEY

BATTERY ENERGY Open Access

RESEARCH ARTICLE OPEN ACCESS

Viologen as an Electrolyte Additive for Extreme Fast Charging of Lithium-Ion Batteries

Murugavel Kathiresan[1] | Abishek Kumar Lakshmi[1] | Natarajan Angulakshmi[2] | Sara Garcia-Ballesteros[3] | Federico Bella[2,3] | A. Manuel Stephan[1]

[1]CSIR-Central Electrochemical Research Institute, Karaikudi, Tamil Nadu, India | [2]GISEL-Consorzio Interuniversitario Nazionale per la Scienza e Tecnologia dei Materiali, Firenze, Italy | [3]Department of Applied Science and Technology, Politecnico di Torino, Turin, Italy

Correspondence: Sara Garcia-Ballesteros (sara.garcia@polito.it) | Federico Bella (federico.bella@polito.it) | A. Manuel Stephan (amstephan@cecri.res.in)

Received: 5 September 2024 | **Revised:** 21 December 2024 | **Accepted:** 16 January 2025

Keywords: electrolyte | fast-charge | lithium-ion battery | lithium-metal battery | viologen

ABSTRACT

Although lithium-ion batteries (LIBs) have found an unprecedented place among portable electronic devices owing to their attractive properties such as high energy density, single cell voltage, long shelf-life, etc., their application in electric vehicles still requires further improvements in terms of power density, better safety, and fast-charging ability (i.e., 15 min charging) for long driving range. The challenges of fast charging of LIBs have limitations such as low lithium-ion transport in the bulk and solid electrode/electrolyte interfaces, which are mainly influenced by the ionic conductivity of the electrolyte. Therefore, electrolyte engineering plays a key role in enhancing the fast-charging capability of LIBs. Here, we synthesize a novel propionic acid-based viologen that contains a 4,4′-bipyridinium unit and a terminal carboxylic acid group with positive charges that confine PF_6^- anions and accelerate the migration of lithium ions due to electrostatic repulsion, thus increasing the overall rate capability. The $LiFePO_4$/Li cells with 0.25% of viologen added to the electrolyte show a discharge capacity of 110 mAh g^{-1} at 6C with 95% of capacity retention even after 500 cycles. The added viologen not only enhances the electrochemical properties, but also significantly reduces the self-extinguishing time.

1 | Introduction

The depletion of fossil fuel resources, current environmental issues, and the progressive replacement of internal combustion engines by electric vehicles (EVs) have immensely accelerated research activities on alternative energy conversion and storage systems with high power and energy densities [1–4]. Unfortunately, the widespread adoption of EVs is still lacking, owing to the issue related to possible distance that can be traveled and the huge charging time of batteries [5–8]. Accordingly, extreme fast charging (XFC) of lithium-ion batteries (LIBs) has been identified as a unique technique that is capable of recharging batteries in a similar amount of time as refueling of state-of-the-art internal combustion engine vehicles, which is estimated to be 10–15 min [9–12]. Although lithium metal has been identified as an ultimate anode material (a sort of "Holy Grail") for high energy density storage devices, owing to its ultrahigh specific capacity of 3860 mAh g^{-1}, low redox potential (−3.040 V vs. standard hydrogen electrode), and noteworthy density of 0.534 g cm^{-3} [13–16], a few challenges such as low Coulombic efficiency and undesirable dendrite growth are impeding the use of this metal [17–19]. In parallel, advancements in this field involve development of new concepts in electrode design [20–23].

State-of-the-art non-aqueous liquid electrolytes comprise a lithium salt, preferably lithium hexafluorophosphate ($LiPF_6$), dissolved in a combination of organic solvents, such as ethylene carbonate and dimethyl carbonate (EC:DMC 1:1 v/v) [24–27]. In this system, the migration of lithium ions is restricted due to

their solvation by coordinating EC molecules, which obviously reduces the Li^+ transference number and also leads to non-uniform deposition of lithium on the anode upon cycling, eventually causing the formation of dendrites [28–31]. Additionally, carbonate solvents, particularly DMC with high vapor pressure, can start a fire, leading to explosions when short circuits accidentally occur [8–10, 32]. Furthermore, the most widely incorporated lithium salt (i.e., $LiPF_6$) decomposes into hydrofluoric acid (HF) in the presence of moisture. On the other hand, the alternative salt lithium bis(trifluoromethanesulfonyl)imide (LiTFSI) is likely to corrode the aluminum current collector at high potential values (> 4 V) [8–10]; this causes delamination of the active materials from the current collector, leading to poor safety and deterioration of LIBs' performance.

The commonly used LIBs based on a lithium-based transition-metal oxide cathode, a graphitic anode, and a non-aqueous liquid electrolyte are therefore unsuitable for extreme fast-charging conditions. When LIBs are charged at high C-rates, various types of polarizations (such as ohmic, concentration, and electrochemical) take place, limiting the performances of active materials and also increasing the depletion of lithium ions, in addition to the generation of a huge amount of heat. The ohmic drop, specifically at low temperature, notably decreases the cell capacity due to early achievement of cut-off voltage. More importantly, the higher charge density accelerates the corrosion of current collectors, which leads to faster capacity fading [33, 34]. In this framework, the electrolyte properties play a decisive role in affecting the performance of LIBs under XFC conditions. Therefore, addressing these challenges by optimizing the composition of the electrolyte is critically important for the successful commercialization of LIBs for EV application [35–38].

In order to tackle these issues, attempts have extensively been made, including replacement of non-aqueous liquid electrolytes by solid polymer electrolytes [39], superionic conductors [40, 41], ionic liquids [42, 43], introduction of super concentrated electrolytes [44–47], electrolyte additives [48, 49], artificial solid electrolyte interphases [50, 51], *etc.* Nevertheless, the poor electrode/electrolyte interfacial properties of superionic conductors and solid polymer electrolytes as well as their processibility still remain major challenges for practical applications. Thus, the incorporation of electrolyte additives (usually 5%–10% by weight or volume) has been identified as a potential strategy to improve the electrochemical performances of LIBs [26, 27]. An incremental improvement in the charging rate of LIBs and lithium-metal batteries has been achieved by using dual-salt electrolytes, e.g., LiTFSI with lithium bis(oxalato)borate [52].

Viologens are organic salts that show redox behavior and, when a bias potential is applied, they undergo reduction in two consecutive steps. However, their highly reactive radical intermediate leads to a number of undesirable side reactions that contribute to comproportionation, dimerization, etc. Viologens are widely investigated systems in supramolecular chemistry, leading to host/guest systems that interact with other molecules via electrostatic interactions, ion–dipole interactions, donor–acceptor interactions, charge-transfer complexation, etc. [53, 54]. Being dicationic salts, viologens show electrostatic attraction with negatively charged species and this has been utilized in Li–S systems to restrict polysulfide migration [55]. Similarly, viologens can confer electrostatic repulsion to lithium ions, which can enhance the mobility of this species and also inhibit dendrite formation [56]. We have investigated these hypotheses and the results are documented [33, 34].

In this study, we have prepared a propionic acid-based viologen that contains a 4,4′-bipyridinium unit and a terminal carboxylic acid group; this species was incorporated as an electrolyte additive to improve the Li^+ transport number and suppress lithium dendrite formation, thereby facilitating fast-charging applications. Enhanced cycling performance of $LiFePO_4$/Li cells by optimizing a non-aqueous electrolyte composed of $LiPF_6$ 1 M in EC:DMC (1:1 v/v) is demonstrated. In order to increase the solubility of viologen and to reduce the viscosity of the electrolyte, acetonitrile was used as a co-solvent; it has oxidation tolerance, a high dielectric constant, and a wide electrochemical stability window (above 5 V), though it has poor reductive stability [57, 58]. The combination of added acetonitrile and viologen not only leads to the formation of a highly stable solid electrolyte interphase (SEI), but also improves the wettability of the membrane, reduces the self-extinguishing time, inhibits aluminum corrosion, and increases the discharge capacity of $LiFePO_4$/Li cells even at a 6C rate.

2 | Results and Discussion

2.1 | Physico-Chemical Characterization and Electrochemical Behavior

The formulation, ionic conductivity, density, viscosity, and lithium-ion transference number of the bare and viologen-added electrolytes were measured at 25°C and are shown in Table 1. There are marginal differences in the values of density and viscosity due to the incorporation of viologen. Although the viologen-added electrolyte was expected to have higher viscosity and density than the bare electrolyte, no discernible changes in these values were observed, as a compensation effect is produced by acetonitrile. However, the value of ionic conductivity is found to be higher for the viologen-added electrolyte.

The contact angle is usually measured by dropping the non-aqueous liquid electrolyte on the polyolefin separator, in order to determine its wettability. In general, poor wettability of the

TABLE 1 | Composition and physicochemical data of the two electrolytes at 25°C.

Sample	Composition	Transport number	Conductivity ($\times 10^{-3}$ S cm^{-1})	Viscosity (mPa s)	Density (g cm^{-3})
Bare	$LiPF_6$ 1 M in EC/DMC 1:1 vol/vol	0.57	0.9	1.398	1.185
Viologen-added	Bare + viologen 0.25 wt% + acetonitrile 1 vol%	0.64	1.1	1.353	1.198

membrane increases the cell resistance and reduces the rate capability. The wettability of the electrolyte with the polyolefin membrane is a direct measure of the contact angle. The contact angle values of the bare and viologen-added electrolytes with the Celgard 2500 membrane are depicted in Supporting Information S1: Figure S1a,b, respectively. The viologen-added electrolyte had a lower contact angle value and showed better wettability than the bare electrolyte, and this was attributed to the hydrophilic nature of viologen-added electrolytes [59, 60].

The conventional LIB electrolytes are highly flammable and the flame lasts for more than 15 s. Extinguishing the flames by the introduction of electrolyte additives or a co-solvent to electrolytes has been found to be an effective strategy as well as economically viable. In general, four types of flame retardants have been explored for LIB applications (i.e., phosphates, phosphides, phosphazene, and fluorinated ethers) [26, 27]. Nevertheless, incorporation of electrolyte additives leads to considerable deterioration in the performance of LIBs, as some of them are incompatible with the electrolyte solvents [61, 62]. Figure 1 shows the self-extinguishing time for the bare electrolyte to be 17 s per 100 μL. On the other hand, upon addition of viologen, the electrolyte is completely extinguished before 7 s per 100 μL. According to Roth and Orendorff [39], two mechanisms can be proposed to explain the role of flame-retardant additives. The first one is the physical char-forming process, where an isolating layer is formed between the condensed and gas phases, whereas the second one is the termination of the chemical combustion process [40]. In the present work, when the added viologen is heated above the pyrolysis temperature, free radicals (i.e., $PO^{\cdot}$ and $F^{\cdot}$) are generated, which actively confine other free radicals generated by the burning electrolytes, such as $H^{\cdot}$ and $OH^{\cdot}$, to inhibit the combustion [63, 64].

In general, fluorinated and/or phosphorous-containing (co-) solvents can suppress the flammability of an electrolyte by means of radical quenching [65]. Upon heating, carbonate-based solvents will produce hydrogen radicals, which will further react with oxygen to produce oxygen-free radicals, which leads to the generation of more free radicals, eventually leading to a self-sustaining fire. One of the effective strategies for terminating this radical formation chain is the introduction of hydrogen or oxygen radical scavengers in the electrolytes. It is well known that fluorinated or phosphorus-containing materials efficiently act as radical scavengers when the electrolyte breaks down. The fluorine and phosphorus radicals, which are electrolyte decomposition products, can react with hydrogen radicals and impede the radical linear chain reaction, which suppresses the combustion of the electrolyte solvent [66]. The typical charge and discharge (voltage vs. specific capacity) profiles obtained at 25°C between 3.45 and 3.4 V versus Li^+/Li at 0.1, 1, 3, and 6C-rates are shown in Supporting Information S1: Figure S2a–d. The cyclic voltammograms of $Li/LiFePO_4$ cells with bare and viologen-added electrolytes are illustrated in Supporting Information S1: Figure S2e, where the $Li/LiFePO_4$ cell with the viologen-added electrolyte shows well-defined and sharp peaks during oxidation and reduction with high amplitude of current. This reveals the fact that the kinetics is faster with viologen-added electrolytes. The $Li/LiFePO_4$ cell showed voltage plateaus at 3.4 V, which are highly reproducible and well defined. The overpotential is also lower at 3- and 6C-rates; the specific capacity approaches almost full capacity, which rapidly reduces to about 155 mAh g^{-1} and, then, it remains almost stable after the 5th cycle.

Figure 2a illustrates the charge–discharge profiles of a $Li/LiFePO_4$ cell with bare and viologen-added electrolytes at different C-rates at 25°C. The formation cycles were performed before charge–discharge studies at higher current densities. The $Li/LiFePO_4$ cells showed voltage plateaus at 3.4 V, which are highly reproducible and well defined. In the cell with bare electrolytes, samples A-1 and A-2 showed an initial discharge capacity of 160 and 176 mAh g^{-1} at a 0.1C-rate during their first cycle, respectively. At a 6C-rate, the $Li/LiFePO_4$ cells showed an initial discharge capacity of 127 and 137 mAh g^{-1}, respectively, with bare and viologen-added electrolytes. The $Li/LiFePO_4$ cells showed a stable discharge capacity up to 500 cycles even at a 6C-rate. On the other hand, an abrupt decrease in the values of discharge capacity for the $Li/LiFePO_4$ cell comprising a bare electrolyte was detected. The capacity decay rates of the cells with bare and viologen-added electrolytes at a 6C-rate were calculated to be 0.1% and 0.03%, respectively. The discharge capacity obtained in the present work is compared with earlier reports and is shown in Supporting Information S1: Table S1.

A similar observation was reported by Zheng et al. [67] for $LiNi_{0.4}Mn_{0.4}Co_{0.2}/Li$ cells. EIS data were recorded before and after cycling (500 cycles) lithium-ion cells with two different electrolytes (i.e., bare and viologen-added electrolytes) at 25°C, and are depicted in Figure 2b,c. The Li-ion cell cycled with a viologen-added electrolyte showed lower solution resistance (R_s) (12.6 Ω) and charge–transfer resistance (R_{ct}) (150.9 Ω) than

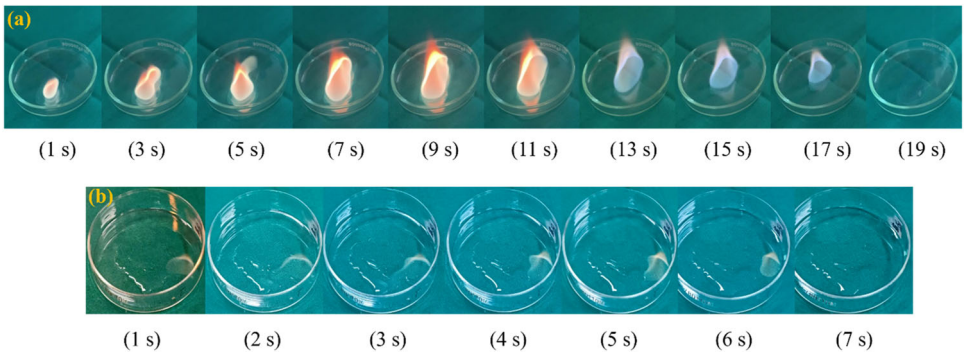

FIGURE 1 | Self-extinguishing time of (a) bare and (b) viologen-added electrolytes at 25°C.

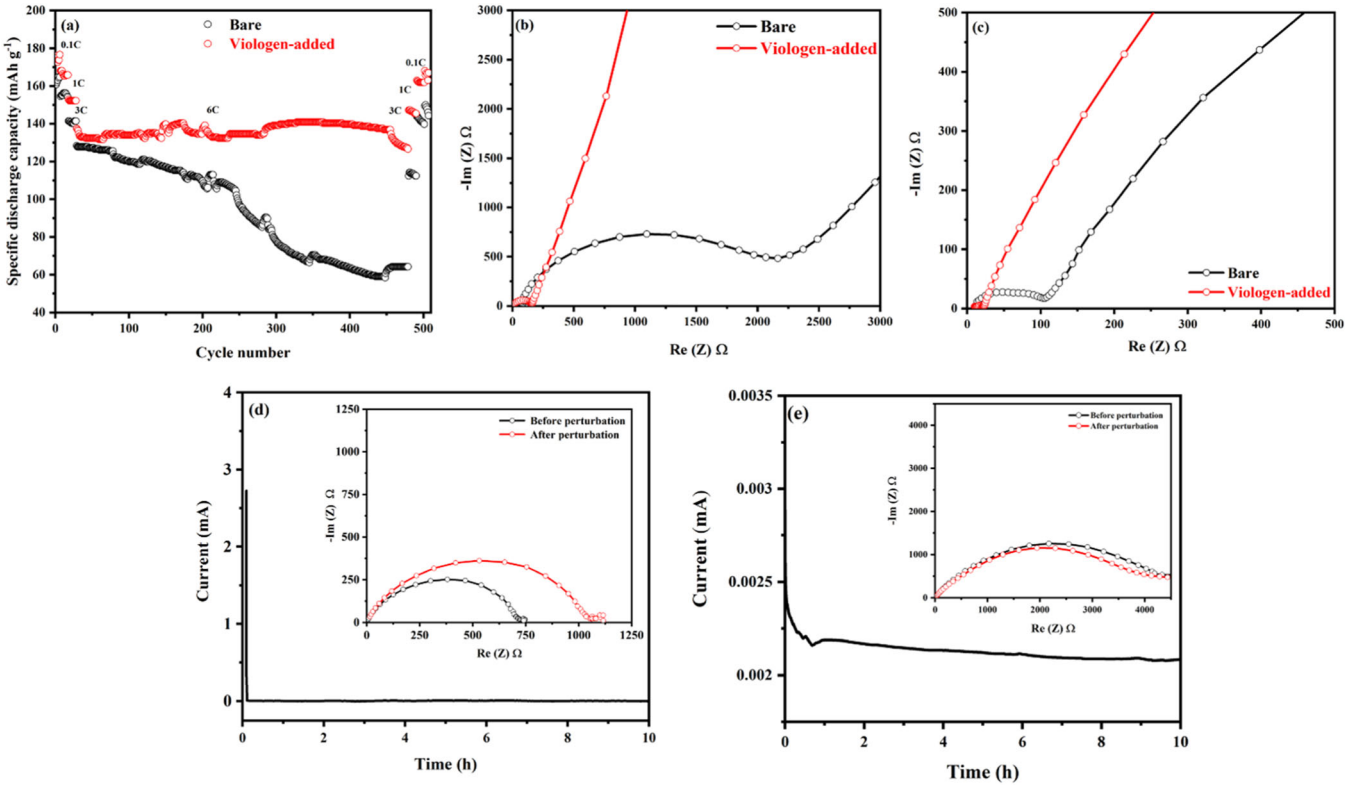

FIGURE 2 | (a) Discharge capacity versus cycle number of $LiFePO_4$//Li cells with viologen-added and bare electrolytes. Data fluctuation is due to issues with the laboratory air conditioning service. EIS plots of $LiFePO_4$//Li cells (b) before and (c) after 500 cycles. Chronoamperometry of a Li/Li symmetric cell with (d) bare electrolytes and (e) viologen-added electrolytes (inset: EIS before and after perturbation).

the cell cycled with a bare electrolyte (i.e., $R_s = 98.4\ \Omega$, $R_{ct} = 1997.9\ \Omega$), which implies that the formed SEI layer has better conductivity due to the added viologen. Upon cycling (500 cycles, Figure 2b), though the values of R_s and R_{ct} were reduced, the value of R_{ct} in the presence of the bare electrolyte was found to be higher and this was attributed to the rapid consumption of the electrolyte due to side reactions with the lithium-metal anode [45]. It is worth mentioning that the values of R_s and R_{ct} are more stable with the viologen-added electrolyte than the bare electrolyte, and this can be ascribed to better compatibility of the viologen-added electrolytes with the lithium-metal anode. This is also substantiated on studying the compatibility of a lithium-metal anode with different electrolytes, as illustrated in Supporting Information S1: Figure S3, where the viologen-added electrolytes showed lower resistance values than the bare electrolytes.

The galvanostatic cycling of a Li/Li symmetric cell configuration at current densities of 0.1 and 0.3 mA cm^{-2} using bare and viologen-added electrolytes is depicted in Supporting Information S1: Figure S4a,b. A dramatic difference was observed between bare and viologen-added electrolytes. For the bare electrolyte, the value of overpotential was high and was attributed to the formation of dead lithium with cycling, resulting in cell failure after 30 h. On the other hand, the Li/Li cells with viologen-added electrolyte showed stable cycling stability and the overpotential remained almost unchanged even after 120 h. As described in the experimental section, the lithium-ion transport number was calculated using Equation (2). The chronoamperometric curves of Li/Li cells with bare and viologen-added cells are illustrated in Figure 2d,e. The values of the lithium-ion transport number were determined to be 0.57 and 0.64, respectively, for the bare and viologen-added electrolytes. An increase in the value of lithium-ion transference number was observed for the viologen-added electrolyte and this was presumably attributed to the confinement of PF_6^- anions by the added viologen ions, as schematically illustrated in Figure 3.

The metallic dendrite nucleation mechanism was proposed in 1901 by Sand, but it is still widely adopted for lithium dendrites and it is often used to obtain its nucleation time [68]. At higher charging rates and with non-aqueous liquid electrolytes, the concentration of cations at the surface of the lithium metal battery electrode will decrease to zero at Sand's time. The nucleation time of lithium dendrites can be calculated using Sand's equation as follows [46]:

$$t_{\text{Sand}} = \frac{\pi \times D_{\text{app}} \times (Z_c \times C_0 \times F)^2}{4 \times (j \times t_a)^2}, \quad (1)$$

where D_{app}, Z_c, C_o, and F represent the apparent diffusion coefficient, the cationic charge number ($Z_c = 1$ for Li^+), the bulk salt concentration, and the Faraday's constant, respectively. Then, j and $t_a = 1 - t_{Li}{}^+$ represent the current density, the transference number of Li^+ and that of associated anions, respectively. Therefore, the prolongation of the nucleation time of dendrites can effectively mitigate the formation of lithium dendrites, which can only be achieved by reducing the current

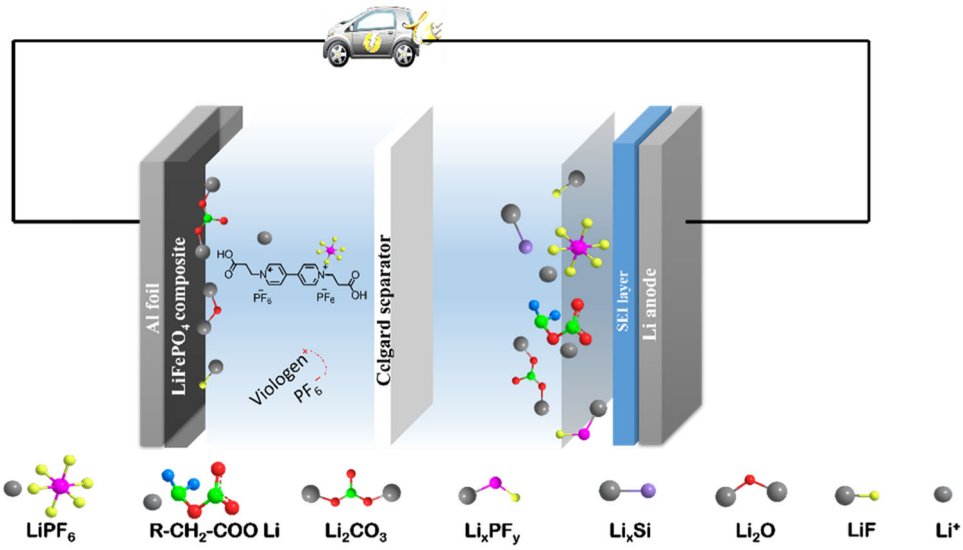

FIGURE 3 | Schematic representation of electrostatic attraction of PF_6^- by added viologen.

density or increasing the t_{Li}^+. This can be accomplished either by the introduction of functional membranes or by modification of the non-aqueous liquid electrolytes. In the present work, viologen with two positive charges is expected to confine the PF_6^- anion due to its electrostatic attraction, and it also accelerates the migration of lithium-ion by electrostatic repulsion. This process enhances the lithium-ion transport number and, thereby, increases the rate capability at the 6C-rate.

Aluminum foil current collectors, which are the main state-of-the-art LIBs, naturally generate Al_2O_3 on their surfaces. However, Al_2O_3 is only resistive enough against corrosion in the normal operation of LIBs [69]. This naturally formed passive layer prevents corrosion of aluminum current collectors at higher potential. Depending on the environmental conditions, the passive films are composed of oxides, oxyhydroxides, and hydroxides that confer an additional benefit, i.e., providing an adhesive property for the coated active materials [70, 71]. Upon long-term storage in the charged state and also while cycling, pitting corrosion of the aluminum current collector has been observed for lithium-metal and LIBs [49]. Moreover, the added lithium salt (i.e., $LiPF_6$) in the non-aqueous liquid electrolyte is highly unstable under some thermal/chemical conditions, which can lead to the production of PF_5, which is a strong Lewis acid that increases the decomposition of electrolyte solvents [72–74]. Furthermore, $LiPF_6$ is prone to undergo hydrolysis, in the presence of water impurities, to produce HF, which obviously degrades the performance of the battery. Several attempts have been made to circumvent this issue by incorporating lithium salts of different anions (e.g., FSA, FSI, $N(SO_2F)_2$) [52, 75].

The aluminum corrosion in batteries causes several issues, e.g.: (i) it passivates cathode active materials, (ii) the formed solid products increase the electrical resistance, and (iii) it contaminates the non-aqueous liquid electrolytes, triggers self-discharge, and the discharged Al^{3+} ions migrate to the anode and are deposited [50]. Incorporation of electrolyte additives is a widely used strategy to prevent aluminum corrosion of LIBs. The addition of fluorinated solvents such as methyl difluoroacetate has been found to suppress the corrosion of aluminum foils and was attributed to the passivation of the aluminum surface due to the generation of AlF_3. Several techniques have been used to investigate the corrosion behavior of aluminum current collectors, which include CV or linear sweep voltammetry, EIS, XPS, SEM, etc. [51–53, 76]. In the present work, potentiodynamic polarization, atomic force microscopy (AFM), SEM, and EIS have been used to probe the corrosion behavior of both aluminum and copper current collectors.

Figure 4 depicts the potentiodynamic polarization curves for an aluminum current collector immersed in a non-aqueous liquid electrolyte for 1, 24, 48, 72, 96, and 120 h. The electrochemical parameters, such as corrosion potential (E_{corr}), corrosion current density (I_{corr}), anodic (ßa) and cathodic (ßc) Tafel slopes, have been calculated from Tafel extrapolation of the polarization plots and are displayed in Table 2. The polarization resistance (R_p) was calculated using Equation (2):

$$R_p = \frac{\beta_a \times \beta_c}{2.303 \times I_{corr} \times (\beta_a + \beta_c)}. \quad (2)$$

When the value of R_p increases, the corrosion rate (CR) decreases, as illustrated in Table 2 and calculated using Equation (3). The value of R_p is found to be higher for the viologen-added electrolytes than the bare electrolyte. Similarly, the corrosion rate was also found to be higher for the bare electrolyte.

$$\mathrm{CR} = \frac{10 \times \text{weight loss of the respected foil (g)}}{\text{density (g cm}^{-3}) \times \text{area (cm}^2) \times \text{time (y)}}. \quad (3)$$

The surface morphology and EDS data are displayed in Supporting Information S1: Figure S5. The surface morphology of the bare aluminum foil shows a rough morphology. Upon immersion in the non-aqueous liquid electrolyte containing viologen for 120 h, cracks are seen on the aluminum surface.

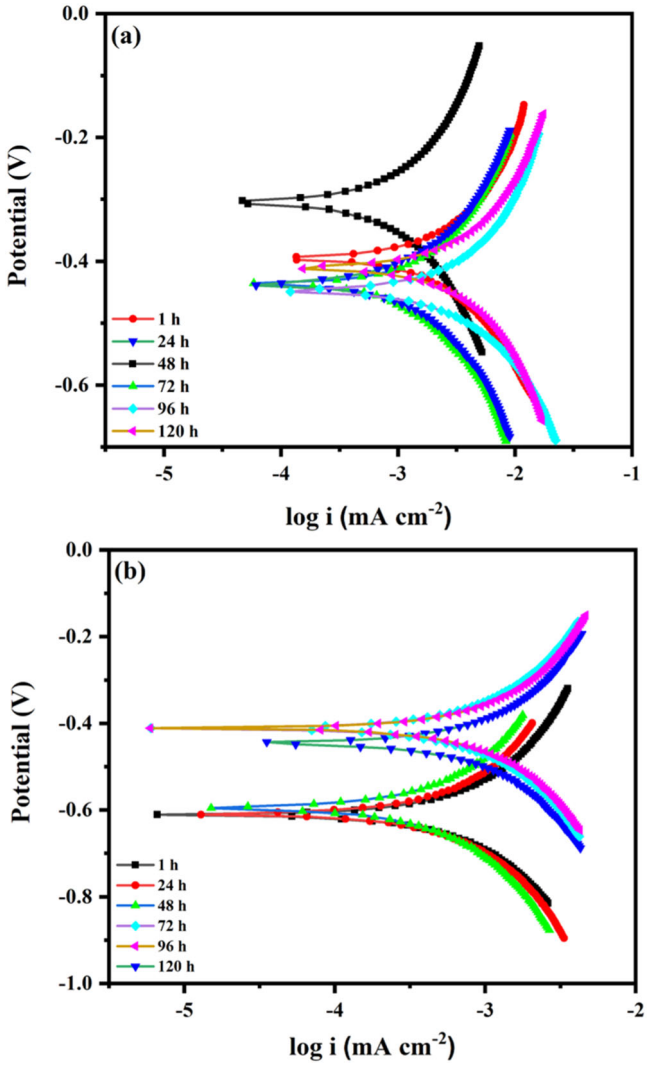

FIGURE 4 | Potentiodynamic polarization curves (Tafel plots) of an aluminum foil soaked in (a) bare and (b) viologen-added electrolytes for different time intervals.

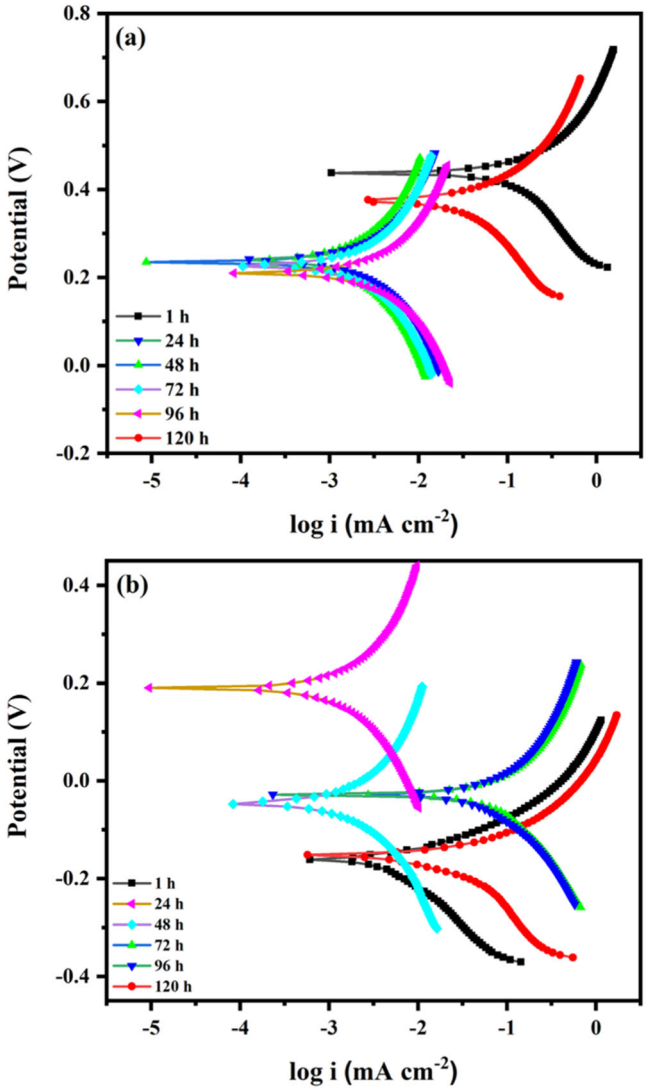

FIGURE 5 | Potentiodynamic polarization curves (Tafel plots) of a copper foil soaked in (a) bare and (b) viologen-added electrolytes for different time intervals.

TABLE 2 | Electrochemical parameters of the potentiodynamic curves of an Al foil in electrolytes with different additives.

Sample	Time	E_{corr} (V)	I_{corr} (μA)	β_a (V dec^{-1})	β_c (V dec^{-1})	R_p (kΩ)	Corrosion rate (mmpy)
Bare	After 1 h	−0.3927	5.23	0.408	0.31	14.63	1.411
	After 1 day	−0.4259	2.697	0.3819	0.4139	31.98	
	After 2 days	−0.3074	2.169	0.4217	0.3952	40.82	
	After 3 days	−0.436	3.249	0.3944	0.4146	27.005	
	After 4 days	−0.4394	4.9	0.4354	0.3488	17.16	
	After 5 days	−0.4053	5.554	0.3879	0.3725	14.85	
Viologen-added	After 1 h	−0.6099	1.2	0.2926	0.276	51.39	0.359
	After 1 day	−0.6044	0.721	0.266	0.361	92.234	
	After 2 days	−0.5965	0.5936	0.2987	0.332	115.02	
	After 3 days	−0.4135	1.295	0.3093	0.345	54.684	
	After 4 days	−0.4074	1.114	0.2517	0.3023	53.534	
	After 5 days	−0.4439	1.413	0.3086	0.3585	50.963	

TABLE 3 | Electrochemical parameters of the potentiodynamic curves of a Cu foil in electrolytes with different additives.

Sample	Time	E_{corr} (V)	I_{corr} (μA)	β_a (V dec^{-1})	β_c (V dec^{-1})	R_p (kΩ)	Corrosion rate (mmpy)
Bare	After 1 h	0.4375	194.3	0.165	0.257	0.225	49.352
	After 1 day	0.2414	2.672	0.219	0.255	19.146	
	After 2 days	0.223	4.79	0.341	0.35	15.657	
	After 3 days	0.2378	5.025	0.266	0.275	11.684	
	After 4 days	0.2151	6.941	0.308	0.37	10.515	
	After 5 days	0.3733	68.9	0.175	0.241	0.639	
Viologen-added	After 1 h	−0.1609	5.856	0.0567	0.1356	2.965	26.061
	After 1 day	0.1898	3.077	0.315	0.34	23.074	
	After 2 days	−0.0473	3.557	0.251	0.256	15.471	
	After 3 days	−0.0289	101	0.1664	0.1685	0.3599	
	After 4 days	−0.0297	102.6	0.187	0.206	0.4148	
	After 5 days	−0.1526	50.3	0.0208	0.2225	0.1642	

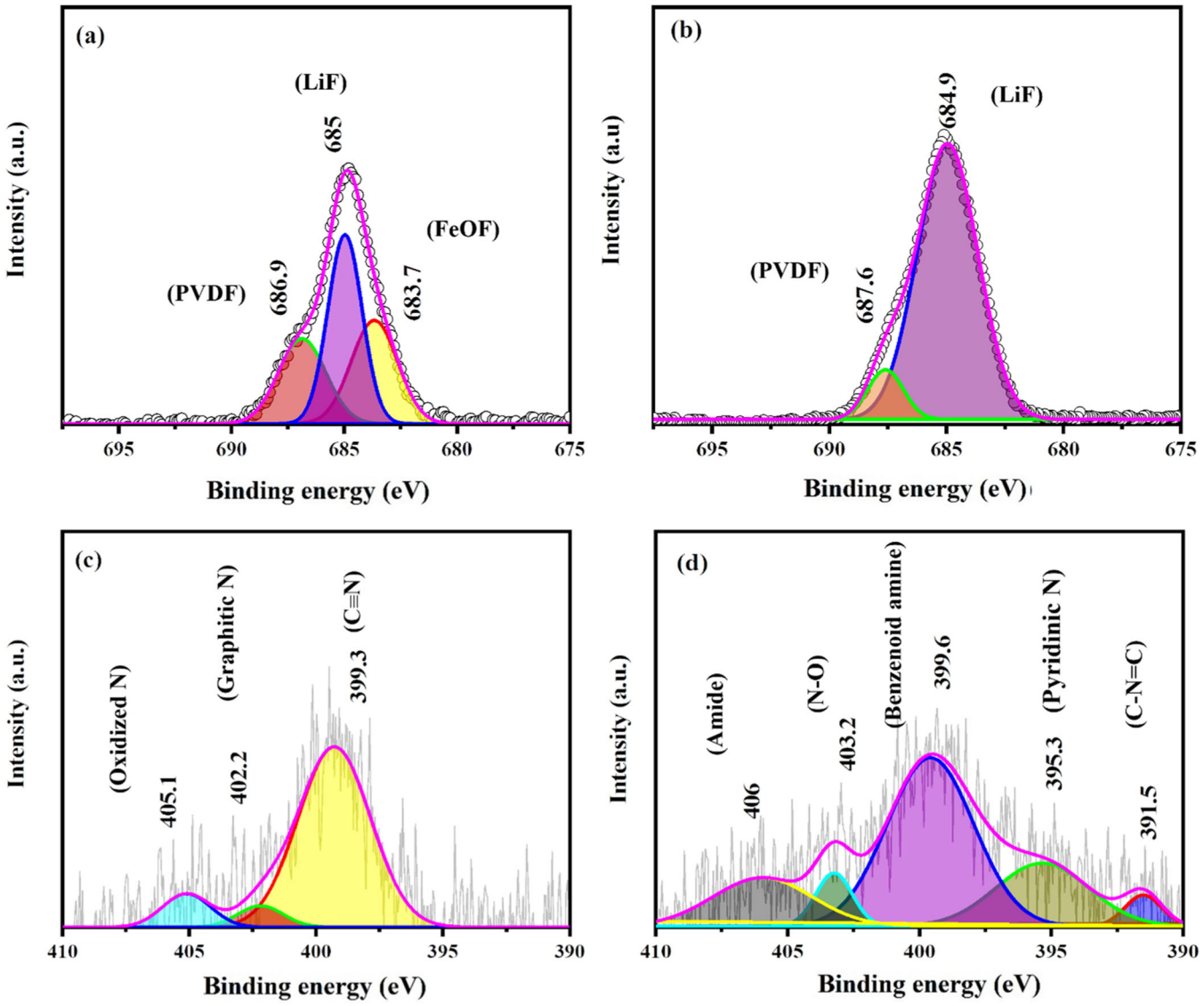

FIGURE 6 | XPS F_{1s} spectra of the cathode surface cycled with (a) bare and (b) viologen-added electrolytes; XPS N_{1s} spectra in the presence of (c) bare and (d) viologen-added electrolytes.

On the other hand, pitting of corrosion is observed on immersion in the bare electrolyte. The corresponding EDS data confirm the presence of phosphorus and fluorine on both surfaces; however, the content of these elements is increased for the aluminum immersed in the bare electrolyte, indicating its more corrosive nature (Supporting Information S1: Figure S5b,c). The formation of F and O elements indicates that the corrosion products are composed of aluminum fluoride and aluminum oxides, as illustrated in the anodic reaction [77–81]. The presence of P further substantiates the formation of AlF_3, as proposed in the cathodic reactions. The AFM images (Supporting Information S1: Figure S6) also illustrate that the surface of the aluminum foil immersed in bare electrolytes is more corroded than when immersed in the viologen-added electrolytes, and also the impedance values further confirm this (Supporting Information S1: Figure S6a,b). Additionally, Table 2 summarizes the impedance values and corrosion rate of an aluminum foil immersed in bare and viologen-added electrolytes (given in mm per year).

The hypothesized mechanism is summarized in the following equations:

Anodic reaction:

$$2Al + 3H_2O \rightarrow Al_2O_3 + 2H^+ + 2e^-, \quad (4)$$

Cathodic reaction:

$$EC + 2e^- + 2Li^+ \rightarrow LiCH_2CH_2OCO_2Li, \quad (5)$$

$$DMC + e^- + Li^+ \rightarrow CH_3^{\cdot} + CH_3OCO_2Li, \quad (6)$$

$$LiPF_6 \leftrightarrow LiF + PF_5, \quad (7)$$

$$PF_5 + H_2O \leftrightarrow 2HF + PF_3O, \quad (8)$$

$$Al_2O_3 + 6HF \leftrightarrow 2AlF_3 + 3H_2O. \quad (9)$$

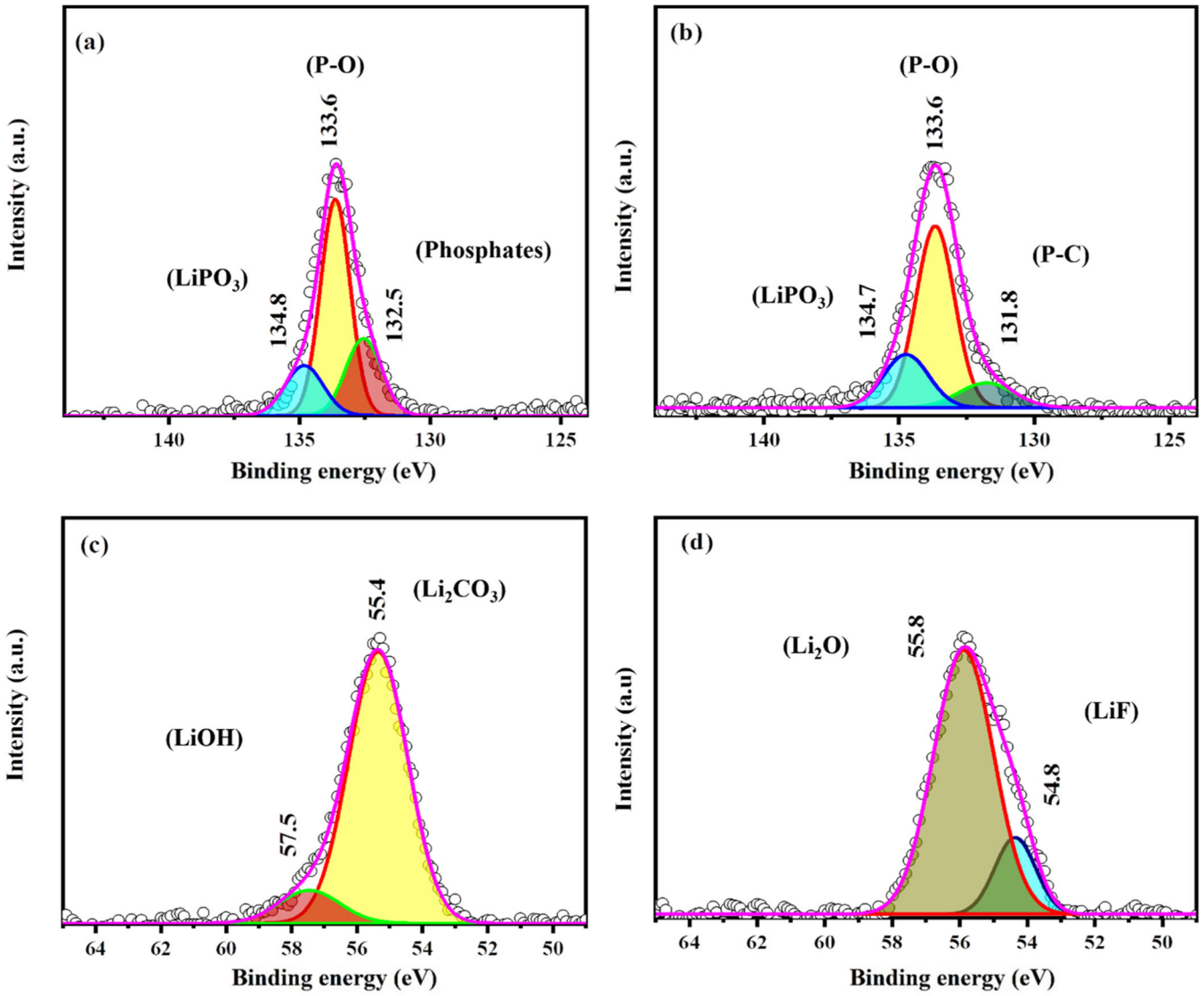

FIGURE 7 | XPS P_{2p} spectra of the cathode surface cycled with (a) bare and (b) viologen-added electrolytes; XPS Li_{1s} spectra in the presence of (c) bare and (d) viologen-added electrolytes.

Similarly, the corrosion behavior of a copper current collector was analyzed and their Tafel plots are displayed in Figure 5.

The anodic reaction is

$$Cu + xH_2O \rightarrow Cu_xO + 2xH^+ + 2xe^-. \quad (10)$$

Oxygen reduction as a cathodic reaction can be neglected in such a closed system; however, EC and DMC in the electrolyte have been reduced to compounds that absorb on the surface of copper, as shown in Equations (5) and (6).

It is worth mentioning that $LiPF_6$ can decompose and react with the traces of water that exist in the electrolyte to subsequently produce HF and PF_3O. The presence of traces of HF in the water residuals results in a significant reduction in the pH. The copper foil can sometimes corrode in a deoxygenated acid solution and the copper oxide can dissolve in the solution containing HF. This results in the reactions described in Equations (7) and (8), as well as in

$$CuO_x + 2xHF \rightarrow CuF_2 + xH_2O. \quad (11)$$

In general, during the electrochemical corrosion process, oxide films are formed and are eventually ruptured [82, 83]. According to Equation (11), galvanic coupling is formed between the attacked copper oxide and the intact sites, which further forms small anodes when metal dissolution occurs. Additionally, the pitting corrosion induced by F occurs on the surface of copper. Moreover, the pH is locally reduced due to the formation of H^+, resulting in the dissolution of copper oxide [84]. With an increase in the concentration of metal ions and accumulation of positive charge, a strong electric field is thus formed, which attracts PF_6^- or decomposed F^- inside the holes. By the synergistic effect of H^+ and F^-, the pitting holes are continuously dissolved by the self-catalyzed effect [85, 86]. Therefore, holes are formed with increasing exposure time. The detected elements P and F in the EDS spectra (Supporting Information S1: Figure S7) in the holes further substantiate this phenomenon. With an increase in the immersion time in the electrolyte, various organic and inorganic compounds are produced by the spontaneous decomposition or electrochemical reduction of the electrolyte solvents (i.e., EC and DMC) deposited on the surface of copper with the formation of a porous

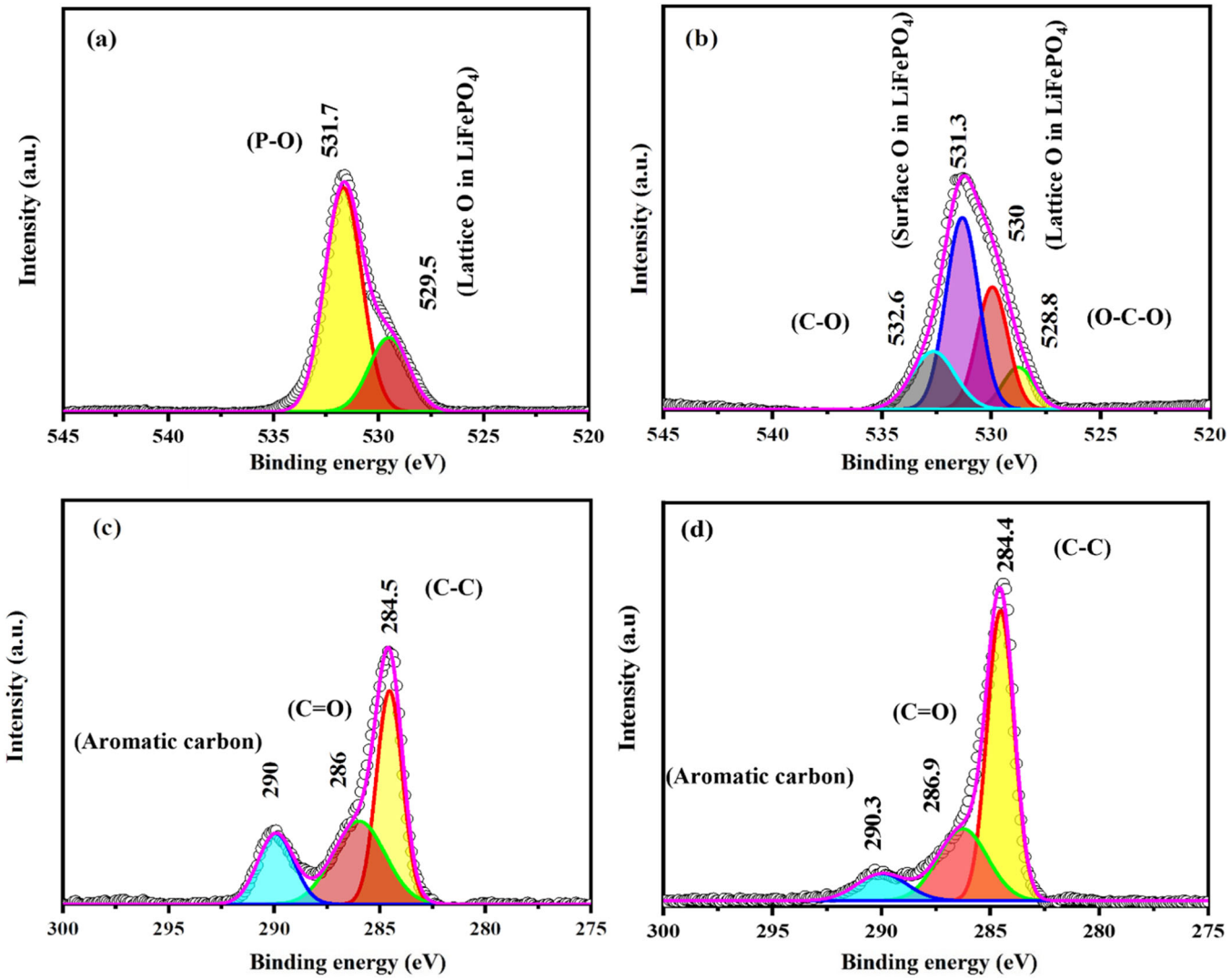

FIGURE 8 | XPS O_{1s} spectra of the cathode surface cycled with (a) bare and (b) viologen-added electrolytes; XPS C_{1s} spectra in the presence of (c) bare and (d) viologen-added electrolytes.

corrosion product layer [56–58]. The AFM images (Supporting Information S1: Figure S8) also illustrate that the surface of the copper foil immersed in bare electrolytes is more corroded than that immersed in the viologen-added electrolyte. Additionally, Table 3 also shows the impedance values and corrosion rate of a copper foil immersed in bare and viologen-added electrolytes (given in mm per year). The prevention of aluminum and copper corrosion due to the viologen-added electrolyte can presumably be attributed to the decomposition of the electrolyte additive (viologen), which prevents electrolyte decomposition and thus prevents HF attack on both current collectors [32].

2.2 | XPS Studies of the Cathode/Electrolyte Interface

In order to investigate the surface properties, cathode samples cycled with bare and viologen-added electrolytes were subjected to XPS and FT-IR analyses. The samples were rinsed thrice with DMC before characterization in order to remove the traces of electrolytes. Supporting Information S1: Figure S15a,b shows the full survey of XPS spectra of bare and viologen-added electrolytes, respectively. Figure 6a–d shows that F_{1s} of the cathode sample cycled with viologen-added electrolyte peaks at 684.9 and 687.6 eV, assigned to LiF and PVDF, respectively. In addition to the typical peaks of LiF and PVDF, an additional peak at 683.7 eV has been observed for the sample cycled with a bare electrolyte, which can be ascribed to the formation of FeOF [57]. In the case of N_{1s} spectra, peaks at 391.5, 395.3, 399.6, 403.2, and 405.9 are, respectively, ascribed to C–N=C, pyridinic linkage, benzenoid amine, oxide-N species, N–O bond, and amide for the sample cycled with viologen-added electrolytes, whereas only three peaks are observed at 399.3, 402.2, and 405.1 eV for the sample cycled with bare electrolytes and are attributed to C ≡ N, graphitic N, and oxidized N, respectively.

Upon cycling, the sample with the bare electrolyte showed three peaks at 132.5 and 133.6 eV (Figure 7a,b), which are assigned to phosphates/P–O, while that at 134.8 eV is attributed to $LiPO_3$. In the case of the electrode cycled with a viologen-added electrolyte, an additional peak was found at 131.8 eV, attributed to P–C. For Li_{1s}, the bare electrolyte showed peaks at 55.4 and 57.5 eV, attributed to Li_2CO_3 and LiOH, respectively (Figure 7c,d). The sample cycled with a viologen-added electrolyte showed peaks at 54.8 and 55.8 eV, attributed to LiF and Li_2O, respectively. In O_{1s} (Figure 8a,b), the peaks observed at 528.8, 530, 531.3, and 532.6 eV are attributed to

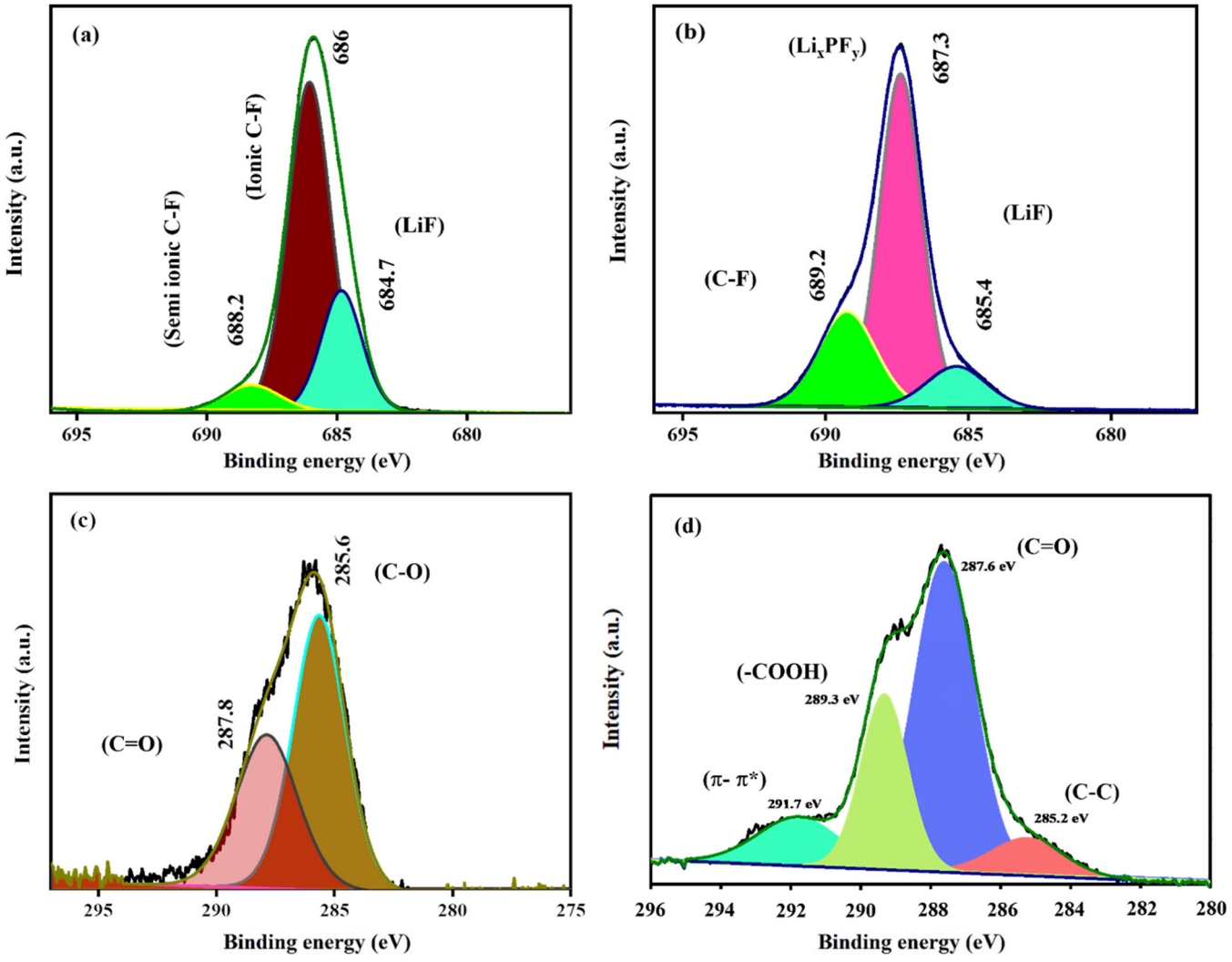

FIGURE 9 | XPS F_{1s} spectra of a lithium surface cycled with (a) bare and (b) viologen-added electrolytes; XPS C_{1s} spectra in the presence of (c) bare and (d) viologen-added electrolytes.

the O–C–O bond originating from $ROCO_2Li$, lattice and surface oxygen in $LiFePO_4$, and oxygen in C–O/P–O–F, respectively, for the cathode material cycled with viologen-added electrolytes. However, the sample cycled with bare electrolytes displayed peaks at 529.5 and 531.7 eV and are ascribed to lattice oxygen in $LiFePO_4$ and the P–O group, respectively. The C_{1s} XPS spectrum of viologen-added sample (Figure 8c,d) showed peaks at 284.4, 286.9, and 290.3, corresponding to C–C, C=O, and aromatic carbon compounds/carboxylate carbon, respectively. Both viologen-added and bare samples displayed peaks corresponding to C–C, C=O, and carboxylate carbons.

2.3 | XPS Studies of the Anode/Electrolyte Interface

The lithium metal anode surfaces cycled with bare and viologen-added electrolytes were characterized by XPS and are displayed in Figures 9–11. The C_{1s} spectra of the anode surface without viologen showed binding energy peaks at 287.8 and 285.6 eV, attributed to C=O and C–O, respectively, whereas the viologen-added anode surface showed binding energy peaks at 291.7, 289.3, 287.6, and 285.2 eV, ascribed to aromatic π–π* transitions/C–F groups, the carboxylic acid (COOH), carbonyl group (C=O), and C–C groups, respectively. Possibly, these peaks can be attributed to the presence of a viologen molecule in the sample. The F_{1s} spectra of the anode surface without viologen showed peaks at 688.2, 686, and 684.7, attributed to semi-ionic and ionic C–F bonds and LiF, respectively. The viologen-added anode surface showed peaks at 689.2, 687.3, and 685.4 eV, attributed to C–F, Li_xPF_y, and LiF formed as a result of the decomposition of the electrolyte. Upon cycling, the sample with the bare electrolyte showed two peaks at 137.8 and 135.1 eV, which are assigned P–F and P–O functional groups, respectively. In the case of the electrode cycled with a viologen-added electrolyte, three distinct peaks at 139.2, 136.5, and 133.4 eV were observed, attributed to $LiPF_6$, Li_xPF_y, and P–O, respectively. The Li_{1s} spectra of the anode without viologen

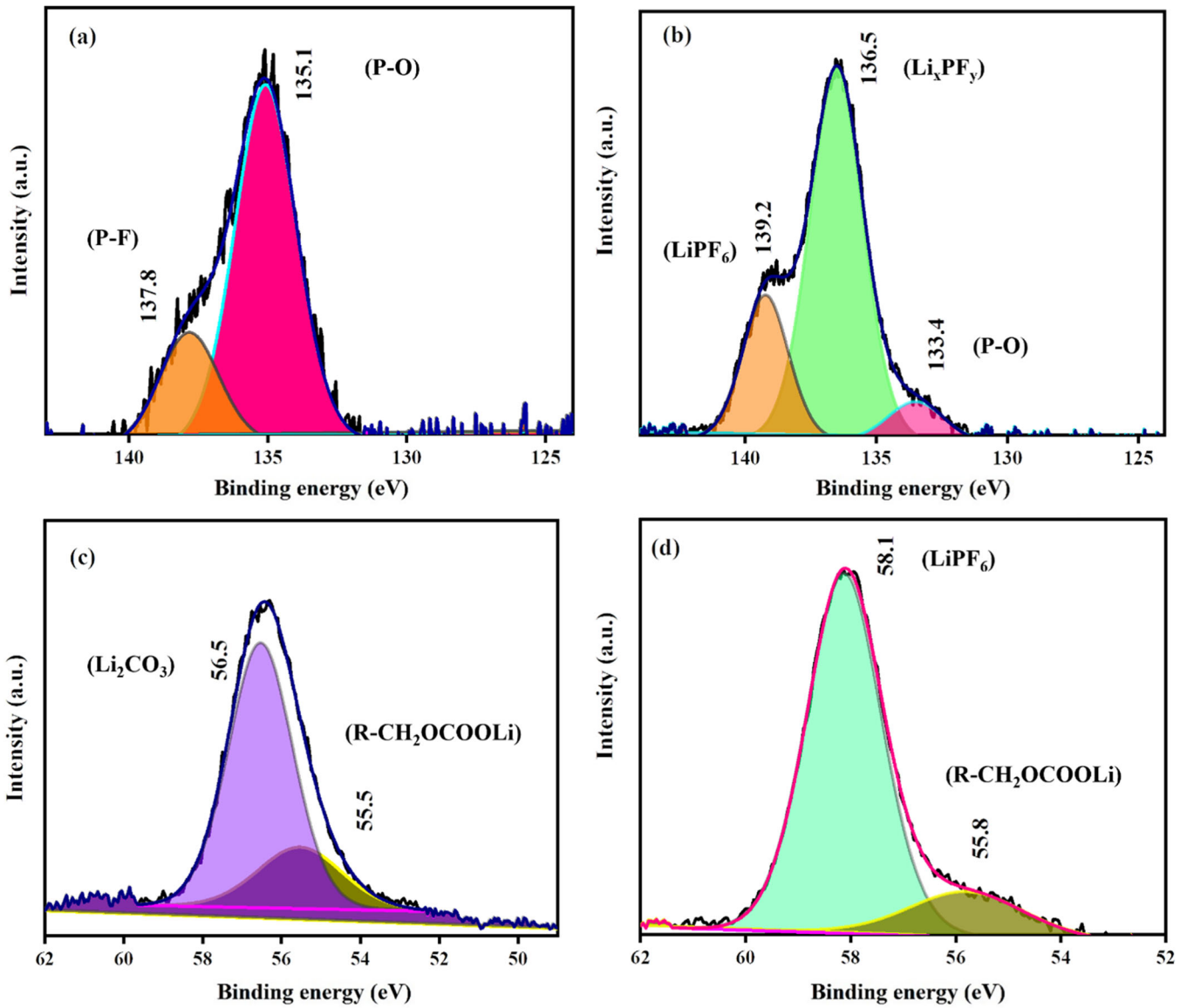

FIGURE 10 | XPS P_{2p} spectra of a lithium surface cycled with (a) bare and (b) viologen-added electrolytes; XPS Li_{1s} spectra in the presence of (c) bare and (d) viologen-added electrolytes.

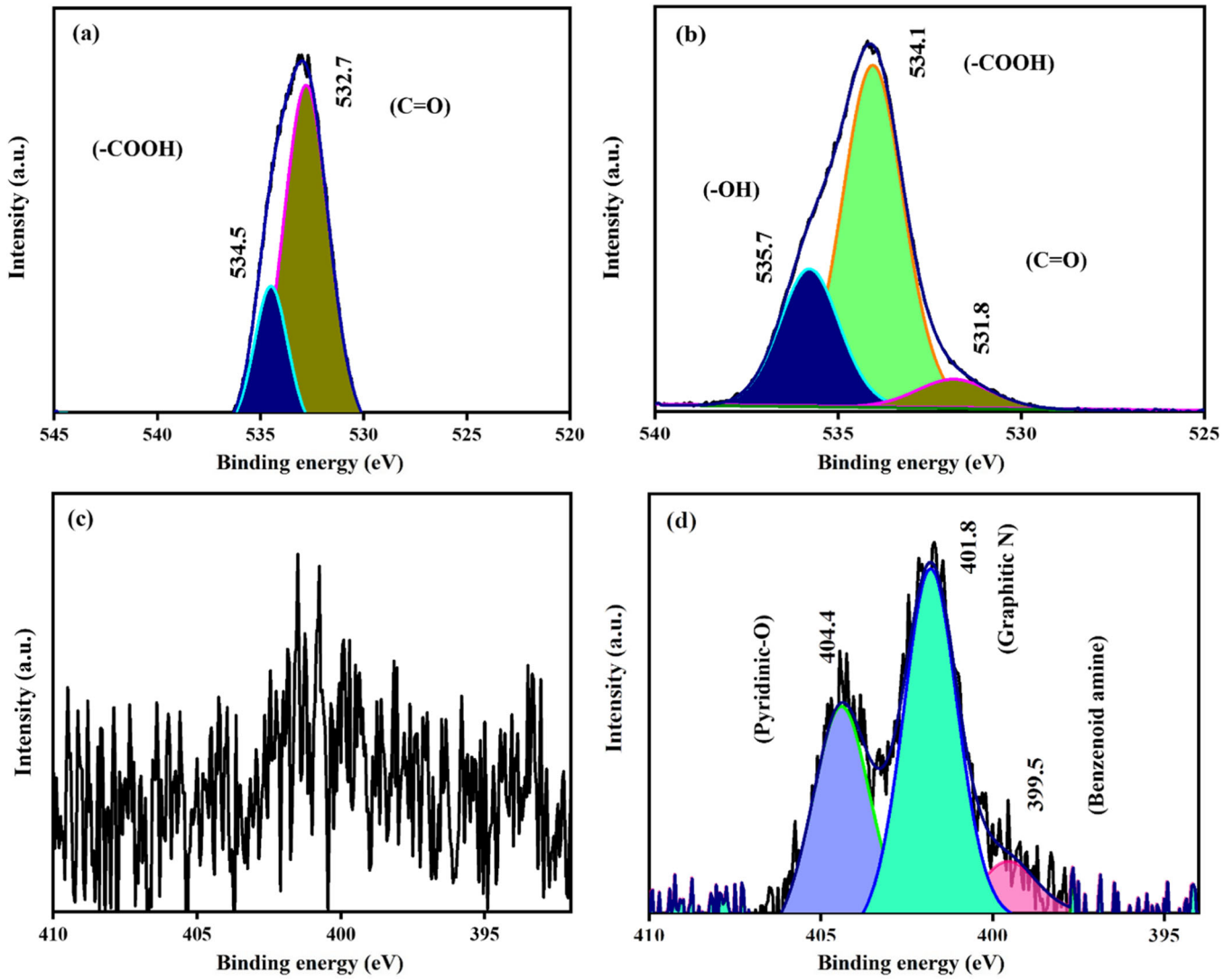

FIGURE 11 | XPS O_{1s} spectra of a lithium surface cycled with (a) bare and (b) viologen-added electrolytes; XPS N_{1s} spectra in the presence of (c) bare and (d) viologen-added electrolytes.

showed two peaks corresponding to Li_2CO_3 and R-CH_2OCOOLi at 56.5 and 55.5 eV, respectively. Likewise, the viologen-added anode showed two peaks at 58.1 and 55.8 eV, attributed to the electrolyte decomposition with Li-rich species (LiF, $LiPF_6$) and formation of R-CH_2OCOOLi, respectively.

The O_{1s} spectra of the anode without viologen showed two peaks corresponding to the oxygen of carboxylic acid and carbonyl groups at 534.5 and 532.7, respectively, whereas the viologen-added anode showed peaks at 535.7, 534.1, and 531.8, attributed to oxygen of the hydroxyl group, carboxylic acid, and the carbonyl group, respectively. This could possibly be attributed to the carboxylic acid terminals present in the viologen. Although the N_{1s} spectra of the anode without viologen did not show any peaks, the viologen-added anode showed three peaks at 404.4, 401.8, and 399.5 eV, attributed to oxidized pyridinic-O, graphitic N, and Benzenoid amine.

Supporting Information S1: Figure S10 shows the FTIR spectra of a lithium surface cycled with bare and viologen-added electrolytes. Although some differences could be seen in the XPS analysis of the cathode/electrolyte and the anode/electrolyte interfaces cycled with bare and viologen-added electrolytes, no discernible changes could be seen in the FTIR spectra. The lithium surfaces showed peaks corresponding to ROCO$_2$Li, Li_2CO_3, aromatic C–H stretching, C–O symmetric and asymmetric stretching bands, and that of P–F stretching, indicating the presence of these functional groups in both cases. The FTIR of the cycled cathode surface showed no significant changes between the bare and viologen-added electrolytes.

3 | Conclusion

We found than an optimal amount of 0.25 wt.% of viologen added in the commercially available electrolyte could considerably enhance the charge–discharge performances of LIBs at a 6C-rate. Stable cycling with an admissible electrode overpotential has been attained at a 6C-rate. The added viologen not only increased the discharge capacity of the $LiFePO_4$/Li cell, but also prevented the corrosion of aluminum and copper current collectors from HF attack. The viologen also minimizes the self-

extinguishing time and thus paves the way for the manufacture of safe and reliable LIBs. The added viologen played a key role in increasing the wettability and facilitating the formation of robust and stable solid electrolyte and cathode/electrolyte interfaces, which are substantiated by XPS analysis.

Author Contributions

M.K., A.M.S., and F.B. conceived the idea. M.K., A.K.L., N.A., and S.G.B. executed the experiments. A.M.S. analyzed the results. All authors equally contributed to manuscript drafting, reading, and approval.

Acknowledgements

M.K., A.K.L., and A.M.S. acknowledge CSIR-Central Electrochemical Research Institute for supporting the publication no. CECRI/PESVC/PUBS/2024-110.

Ethics Statement

The authors have nothing to report.

Conflicts of Interest

The authors declare no conflicts of interest.

Data Availability Statement

The data that support the findings of this study are available from the corresponding author upon reasonable request.

References

1. T. Kim, W. Song, D.-Y. Son, L. K. Ono, and Y. Qi, "Lithium-Ion Batteries: Outlook on Present, Future, and Hybridized Technologies," *Journal of Materials Chemistry A* 7, no. 7 (2019): 2942–2964.

2. J. B. Goodenough and Y. Kim, "Challenges for Rechargeable Li Batteries," *Chemistry of Materials* 22, no. 3 (2010): 587–603.

3. B. Dunn, H. Kamath, and J.-M. Tarascon, "Electrical Energy Storage for the Grid: A Battery of Choices," *Science* 334, no. 6058 (2011): 928–935.

4. J. B. Goodenough and H. Gao, "A Perspective on the Li-Ion Battery," *Science China Chemistry* 62, no. 12 (2019): 1555–1556.

5. L. Qiao, X. Judez, T. Rojo, M. Armand, and H. Zhang, "Polymer Electrolytes for Sodium Batteries," *Journal of the Electrochemical Society* 167, no. 7 (2020): 070534.

6. O. Eroglu, M. S. Kiai, and H. Kizil, "Performance Enhancement of Li-S Battery With the Anatase Nano Structured Fe Doped TiO2 as a Robust Interlayer," *Journal of Alloys and Compounds* 838 (2020): 155607.

7. E. Fedeli, O. Garcia-Calvo, T. Thieu, et al., "Nanocomposite Solid Polymer Electrolytes Based on Semi-Interpenetrating Hybrid Polymer Networks for High Performance Lithium Metal Batteries," *Electrochimica Acta* 353 (2020): 136481.

8. Z. Li, N. Qiao, J. Nie, et al., "NiO/$NiFe_2O_4$ Nanocubes Derived From Prussian Blue as Anode Materials for Li-Ion Batteries," *Materials Letters* 275 (2020): 128077.

9. Z. Wang, H. Zhou, C. Meng, et al., "Enhancing Ion Transport: Function of Ionic Liquid Decorated MOFs in Polymer Electrolytes for All-Solid-State Lithium Batteries," *ACS Applied Energy Materials* 3, no. 5 (2020): 4265–4274.

10. K. Chelladurai, P. Venkatachalam, S. Rengapillai, W.-R. Liu, C.-H. Huang, and S. Marimuthu, "Effect of Polyaniline on Sulfur/Sepiolite Composite Cathode for Lithium-Sulfur Batteries," *Polymers* 12, no. 4 (2020): 755.

11. J. Wu, X. Wu, W. Wang, et al., "Dense PVDF-Type Polymer-In-Ceramic Electrolytes for Solid State Lithium Batteries," *RSC Advances* 10, no. 38 (2020): 22417–22421.

12. Z. Wang, H. Zhou, C. Meng, L. Zhang, Y. Cai, and A. Yuan, "Anion-Immobilized and Fiber-Reinforced Hybrid Polymer Electrolyte for Advanced Lithium-Metal Batteries," *ChemElectroChem* 7, no. 12 (2020): 2660–2664.

13. M. Liu, Y. Wang, M. Li, et al., "A New Composite Gel Polymer Electrolyte Based on Matrix of PEGDA With High Ionic Conductivity for Lithium-Ion Batteries," *Electrochimica Acta* 354 (2020): 136622.

14. G. Chen, K. Zhang, Y. Liu, et al., "Flame-Retardant Gel Polymer Electrolyte and Interface for Quasi-Solid-State Sodium Ion Batteries," *Chemical Engineering Journal* 401 (2020): 126065.

15. X. Zhang, J.-C. Daigle, and K. Zaghib, "Comprehensive Review of Polymer Architecture for All-Solid-State Lithium Rechargeable Batteries," *Materials* 13, no. 11 (2020): 2488.

16. J. Cui, Z. Zhou, M. Jia, et al., "Solid Polymer Electrolytes With Flexible Framework of SiO_2 Nanofibers for Highly Safe Solid Lithium Batteries," *Polymers* 12, no. 6 (2020): 1324.

17. X.-B. Cheng, R. Zhang, C.-Z. Zhao, and Q. Zhang, "Toward Safe Lithium Metal Anode in Rechargeable Batteries: A Review," *Chemical Reviews* 117, no. 15 (2017): 10403–10473.

18. W. Xu, J. Wang, F. Ding, et al., "Lithium Metal Anodes for Rechargeable Batteries," *Energy & Environmental Science* 7, no. 2 (2014): 513–537.

19. J.-M. Tarascon and M. Armand, "Issues and Challenges Facing Rechargeable Lithium Batteries," *Nature* 414, no. 6861 (2001): 359–367.

20. S. N. Lauro, J. N. Burrow, and C. B. Mullins, "Restructuring the Lithium-Ion Battery: A Perspective on Electrode Architectures," *eScience* 3 (2023): 100152.

21. X. Zhang, B. Peng, L. Zhao, et al., "NASICON-Structured $LiZr_2(PO_4)_3$ Surface Modification Improves Ionic Conductivity and Structural Stability of $LiCoO_2$ for a Stable 4.6 V Cathode," *ACS Applied Materials & Interfaces* 14 (2022): 16204–16213.

22. G. Wang, J. Li, L. Yu, J. Gao, and G. Zhang, "Hierarchical Carbon Nanosheet Assembly With SiO_x Incorporation and Nitrogen Doping Achieves Enhanced Lithium Ion Storage Performance," *Advanced Energy and Sustainability Research* 2 (2021): 2100026.

23. J. Gao, Y. Li, L. Shi, J. Li, and G. Zhang, "Rational Design of Hierarchical Nanotubes Through Encapsulating $CoSe_2$ Nanoparticles Into $MoSe_2$/C Composite Shells With Enhanced Lithium and Sodium Storage Performance," *ACS Applied Materials & Interfaces* 10 (2018): 20635–20642.

24. S. Lou, F. Zhang, C. Fu, et al., "Interface Issues and Challenges in All-Solid-State Batteries: Lithium, Sodium, and Beyond," *Advanced Materials* 33 (2021): 2000721.

25. C. Li, L. Liu, J. Kang, et al., "Pristine MOF and COF Materials for Advanced Batteries," *Energy Storage Materials* 31 (2020): 115–134.

26. F. Wu, G.-T. Kim, T. Diemant, et al., "Reducing Capacity and Voltage Decay of Co-Free $Li_{1.2}Ni_{0.2}Mn_{0.6}O_2$ as Positive Electrode Material for Lithium Batteries Employing an Ionic Liquid-Based Electrolyte," *Advanced Energy Materials* 10 (2020): 2001830.

27. S. A. Ahmed, T. Pareek, S. Dwivedi, M. Badole, and S. Kumar, "$LiSn_2(PO_4)_3$-Based Polymer-In-Ceramic Composite Electrolyte With High Ionic Conductivity for All-Solid-State Lithium Batteries," *Journal of Solid State Electrochemistry* 24 (2020): 2407–2417.

28. K. Xu, "Nonaqueous Liquid Electrolytes for Lithium-Based Rechargeable Batteries," *Chemical Reviews* 104, no. 10 (2004): 4303–4418.

29. T. Kawamura, A. Kimura, M. Egashira, S. Okada, and J.-I. Yamaki, "Thermal Stability of Alkyl Carbonate Mixed-Solvent Electrolytes for Lithium Ion Cells," *Journal of Power Sources* 104, no. 2 (2002): 260–264.

30. J. Foropoulos, Jr. and D. D. Desmarteau, "Synthesis, Properties, and Reactions of Bis((Trifluoromethyl)Sulfonyl) Imide (CF3SO2)2NH," *Inorganic Chemistry* 23, no. 23 (1984): 3720–3723.

31. X. Wang, J. Sun, C. Feng, et al., "Lithium Bis(Oxalate)Borate Crosslinked Polymer Electrolytes for High-Performance Lithium Batteries," *Journal of Energy Chemistry* 55 (2021): 228–235.

32. K. Zhou, S. Wang, S. Zhang, F. Kang, and B. Li, "Investigating the Increased-Capacity Mechanism of Porous Carbon Materials in Lithium-Ion Batteries," *Journal of Materials Chemistry A* 8, no. 28 (2020): 14031–14042.

33. E. R. Logan and J. R. Dahn, "Electrolyte Design for Fast-Charging Li-Ion Batteries," *Trends in Chemistry* 2, no. 4 (2020): 354–366.

34. D. Lv, Y. Shao, T. Lozano, et al., "Failure Mechanism for Fast-Charged Lithium Metal Batteries With Liquid Electrolytes," *Advanced Energy Materials* 5, no. 3 (2015): 1400993.

35. A. Nyman, T. G. Zavalis, R. Elger, M. Behm, and G. Lindbergh, "Analysis of the Polarization in a Li-Ion Battery Cell by Numerical Simulations," *Journal of the Electrochemical Society* 157, no. 11 (2010): A1236–A1246.

36. K. G. Gallagher, S. E. Trask, C. Bauer, et al., "Optimizing Areal Capacities Through Understanding the Limitations of Lithium-Ion Electrodes," *Journal of the Electrochemical Society* 163, no. 2 (2016): A138–A149.

37. S. Ahmed, I. Bloom, A. N. Jansen, et al., "Enabling Fast Charging – A Battery Technology Gap Assessment," *Journal of Power Sources* 367 (2017): 250–262.

38. Y. Liu, Y. Zhu, and Y. Cui, "Challenges and Opportunities Towards Fast-Charging Battery Materials," *Nature Energy* 4, no. 7 (2019): 540–550.

39. C. Gerbaldi, J. R. Nair, M. A. Kulandainathan, et al., "Innovative High Performing Metal Organic Framework (MOF)-Laden Nanocomposite Polymer Electrolytes for All-Solid-State Lithium Batteries," *Journal of Materials Chemistry A: Materials for Energy and Sustainability* 2, no. 26 (2014): 9948–9954.

40. N. Kamaya, K. Homma, Y. Yamakawa, et al., "A Lithium Superionic Conductor," *Nature Materials* 10, no. 9 (2011): 682–686.

41. L. Zhou, A. Assoud, Q. Zhang, X. Wu, and L. F. Nazar, "New Family of Argyrodite Thioantimonate Lithium Superionic Conductors," *Journal of the American Chemical Society* 141, no. 48 (2019): 19002–19013.

42. K. Liu, Z. Wang, L. Shi, S. Jungsuttiwong, and S. Yuan, "Ionic Liquids for High Performance Lithium Metal Batteries," *Journal of Energy Chemistry* 59 (2021): 320–333.

43. H. Qi, Y. Ren, S. Guo, et al., "High-Voltage Resistant Ionic Liquids for Lithium-Ion Batteries," *ACS Applied Materials & Interfaces* 12, no. 1 (2020): 591–600.

44. C. M. Efaw, Q. Wu, N. Gao, et al., "Localized High-Concentration Electrolytes Get More Localized Through Micelle-Like Structures," *Nature Materials* 22, no. 12 (2023): 1531–1539.

45. X. Cao, H. Jia, W. Xu, and J.-G. Zhang, "Review-Localized High-Concentration Electrolytes for Lithium Batteries," *Journal of the Electrochemical Society* 168, no. 1 (2021): 010522.

46. L. Suo, Y.-S. Hu, H. Li, M. Armand, and L. Chen, "A New Class of Solvent-in-Salt Electrolyte for High-Energy Rechargeable Metallic Lithium Batteries," *Nature Communications* 4 (2013): 1481.

47. L. E. Camacho-Forero, T. W. Smith, and P. B. Balbuena, "Effects of High and Low Salt Concentration in Electrolytes at Lithium-Metal Anode Surfaces," *Journal of Physical Chemistry C* 121, no. 1 (2017): 182–194.

48. H. Zhang, G. G. Eshetu, X. Judez, C. Li, L. M. Rodriguez-Martínez, and M. Armand, "Electrolyte Additives for Lithium Metal Anodes and Rechargeable Lithium Metal Batteries: Progress and Perspectives," *Angewandte Chemie International Edition* 57, no. 46 (2018): 15002–15027.

49. S. S. Zhang, "A Review on Electrolyte Additives for Lithium-Ion Batteries," *Journal of Power Sources* 162, no. 2 SPEC. ISS (2006): 1379–1394.

50. L. Wang, Q. Wang, W. Jia, S. Chen, P. Gao, and J. Li, "Li Metal Coated With Amorphous Li_3PO_4 via Magnetron Sputtering for Stable and Long-Cycle Life Lithium Metal Batteries," *Journal of Power Sources* 342 (2017): 175–182.

51. J. Zhao, L. Liao, F. Shi, et al., "Surface Fluorination of Reactive Battery Anode Materials for Enhanced Stability," *Journal of the American Chemical Society* 139, no. 33 (2017): 11550–11558.

52. H. Xiang, P. Shi, P. Bhattacharya, et al., "Enhanced Charging Capability of Lithium Metal Batteries Based on Lithium Bis (Trifluoromethanesulfonyl)Imide-Lithium Bis(Oxalato)Borate Dual-Salt Electrolytes," *Journal of Power Sources* 318 (2016): 170–177.

53. M. Kathiresan, B. Ambrose, N. Angulakshmi, D. E. Mathew, D. Sujatha, and A. M. Stephan, "Viologens: A Versatile Organic Molecule for Energy Storage Applications," *Journal of Materials Chemistry A* 9, no. 48 (2021): 27215–27233.

54. K. R. Prakasha, K. Madasamy, M. Kathiresan, and A. S. Prakash, "Ethylviologen Hexafluorophosphate as Electrolyte Additive for High-Voltage Nickel-Rich Layered Cathode," *Journal of Physical Chemistry C* 123, no. 47 (2019): 28604–28610.

55. N. Angulakhsmi, B. Ambrose, S. Sathya, et al., "Enhanced Electrochemical Performance of Hybrid Solid Polymer Electrolytes Encompassing Viologen for All-Solid-State Lithium Polymer Batteries," *ACS Materials Au* 3, no. 5 (2023): 528–539.

56. S. Suriyakumar, K. Madasamy, M. Kathiresan, M. H. Alkordi, and A. M. Stephan, "Improved Cycling Performance of Lithium-Sulfur Cell Through Supramolecular Interactions," *Journal of Physical Chemistry C* 122, no. 49 (2018): 27843–27849.

57. Y. Yamada, K. Furukawa, K. Sodeyama, et al., "Unusual Stability of Acetonitrile-Based Superconcentrated Electrolytes for Fast-Charging Lithium-Ion Batteries," *Journal of the American Chemical Society* 136, no. 13 (2014): 5039–5046.

58. N. Matsuoka, H. Kamine, Y. Natsume, and A. Yoshino, "Moderately Concentrated Acetonitrile-Containing Electrolytes With High Ionic Conductivity for Durability-Oriented Lithium-Ion Batteries," *ChemElectroChem* 8, no. 16 (2021): 3095–3104.

59. J.-H. Park, W. Park, J. H. Kim, et al., "Close-Packed Poly(Methyl Methacrylate) Nanoparticle Arrays-Coated Polyethylene Separators for High-Power Lithium-Ion Polymer Batteries," *Journal of Power Sources* 196, no. 16 (2011): 7035–7038.

60. J.-Y. Sohn, J.-S. Im, J. Shin, and Y.-C. Nho, "PVDF-HFP/PMMA-Coated PE Separator for Lithium Ion Battery," *Journal of Solid State Electrochemistry* 16, no. 2 (2012): 551–556.

61. E. P. Roth and C. J. Orendorff, "How Electrolytes Influence Battery Safety," *Interface Magazine* 21, no. 2 (2012): 45–49.

62. J. Wang, F. Lin, H. Jia, J. Yang, C. W. Monroe, and Y. Nuli, "Towards a Safe Lithium-Sulfur Battery With a Flame-Inhibiting Electrolyte and a Sulfur-Based Composite Cathode," *Angewandte Chemie International Edition* 53, no. 38 (2014): 10099–10104.

63. K. Xu, S. Zhang, J. L. Allen, and T. R. Jow, "Nonflammable Electrolytes for Li-Ion Batteries Based on a Fluorinated Phosphate," *Journal of the Electrochemical Society* 149, no. 8 (2002): A1079–A1082.

64. S. S. Zhang, K. Xu, and T. R. Jow, "A Thermal Stabilizer for $LIPF_6$-Based Electrolytes of Li-Ion Cells," *Electrochemical and Solid-State Letters* 5, no. 9 (2002): A206–A208.

65. G. Nagasubramanian and K. Fenton, "Reducing Li-Ion Safety Hazards through Use of Non-Flammable Solvents and Recent Work at Sandia National Laboratories," *Electrochimica Acta* 101 (2013): 3–10.

66. H. F. Xiang, H. Y. Xu, Z. Z. Wang, and C. H. Chen, "Dimethyl Methylphosphonate (DMMP) as an Efficient Flame Retardant Additive for the Lithium-Ion Battery Electrolytes," *Journal of Power Sources* 173, no. 1 (2007): 562–564.

67. J. Zheng, M. H. Engelhard, D. Mei, et al., "Electrolyte Additive Enabled Fast Charging and Stable Cycling Lithium Metal Batteries," *Nature Energy* 2, no. 3 (2017): 17012.

68. P. Bai, J. Li, F. R. Brushett, and M. Z. Bazant, "Transition of Lithium Growth Mechanisms in Liquid Electrolytes," *Energy & Environmental Science* 9, no. 10 (2016): 3221–3229.

69. T. C. Hyams, J. Go, and T. M. Devine, "Corrosion of Aluminum Current Collectors in High-Power Lithium-Ion Batteries for Use in Hybrid Electric Vehicles," *Journal of the Electrochemical Society* 154, no. 8 (2007): C390–C396.

70. S. Zhang, M. S. Ding, and T. R. Jow, "Self-Discharge of $Li/Li_xMn_2O_4$ Batteries in Relation to Corrosion of Aluminum Cathode Substrates," *Journal of Power Sources* 102, no. 1–2 (2001): 16–20.

71. J. W. Braithwaite, A. Gonzales, G. Nagasubramanian, et al., "Corrosion of Lithium-Ion Battery Current Collectors," *Journal of the Electrochemical Society* 146, no. 2 (1999): 448–456.

72. L. Cong, J. Liu, M. Armand, et al., "Role of Perfluoropolyether-Based Electrolytes in Lithium Metal Batteries: Implication for Suppressed Al Current Collector Corrosion and the Stability of Li Metal/Electrolytes Interfaces," *Journal of Power Sources* 380 (2018): 115–125.

73. B. Philippe, R. Dedryvère, M. Gorgoi, H. Rensmo, D. Gonbeau, and K. Edström, "Improved Performances of Nanosilicon Electrodes Using the Salt Lifsi: A Photoelectron Spectroscopy Study," *Journal of the American Chemical Society* 135, no. 26 (2013): 9829–9842.

74. L. Zhang, L. Chai, L. Zhang, et al., "Synergistic Effect Between Lithium Bis(Fluorosulfonyl)Imide (LiFSI) and Lithium Bis-Oxalato Borate (LiBOB) Salts in $LiPF_6$-Based Electrolyte for High-Performance Li-Ion Batteries," *Electrochimica Acta* 127 (2014): 39–44.

75. M. Zhao, S. Kariuki, H. D. Dewald, et al., "Electrochemical Stability of Copper in Lithium-Ion Battery Electrolytes," *Journal of the Electrochemical Society* 147, no. 8 (2000): 2874–2879.

76. J. Shu, M. Shui, F. Huang, et al., "Comparative Study on Surface Behaviors of Copper Current Collector in Electrolyte for Lithium-Ion Batteries," *Electrochimica Acta* 56, no. 8 (2011): 3006–3014.

77. D. Aurbach, I. Weissman, A. Zaban, and P. Dan, "On the Role of Water Contamination in Rechargeable Li Batteries," *Electrochimica Acta* 45, no. 7 (1999): 1135–1140.

78. G. Ning, R. E. White, and B. N. Popov, "A Generalized Cycle Life Model of Rechargeable Li-Ion Batteries," *Electrochimica Acta* 51, no. 10 (2006): 2012–2022.

79. S. Dai, J. Chen, Y. Ren, et al., "Electrochemical Corrosion Behavior of the Copper Current Collector in the Electrolyte of Lithium-Ion Batteries," *International Journal of Electrochemical Science* 12, no. 11 (2017): 10589–10598.

80. G. Ning, B. Haran, and B. N. Popov, "Capacity Fade Study of Lithium-Ion Batteries Cycled at High Discharge Rates," *Journal of Power Sources* 117, no. 1–2 (2003): 160–169.

81. S.-T. Myung, Y. Sasaki, S. Sakurada, Y.-K. Sun, and H. Yashiro, "Electrochemical Behavior of Current Collectors for Lithium Batteries in Non-Aqueous Alkyl Carbonate Solution and Surface Analysis by Tof-Sims," *Electrochimica Acta* 55, no. 1 (2009): 288–297.

82. A. M. Eldesoky, M. A. Diab, A. A. El-Bindary, A. Z. El-Sonbati, and H. A. Seyam, "Some Antipyrine Derivatives as Corrosion Inhibitors for Copper in Acidic Medium: Experimental and Quantum Chemical Molecular Dynamics Approach," *Journal of Materials and Environmental Science* 6, no. 8 (2015): 2148–2165.

83. A. S. Fouda, A. M. Eldesoky, A. Z. El-Sonbati, and S. F. Salam, "Prop-2-en-1-One Derivatives as Corrosion Inhibitors for Copper in 1 M HNO_3," *International Journal of Electrochemical Science* 9, no. 4 (2014): 1867–1891.

84. N. N. Sinha, J. C. Burns, and J. R. Dahn, "Storage Studies on Li/Graphite Cells and the Impact of So-Called SEI-Forming Electrolyte Additives," *Journal of the Electrochemical Society* 160, no. 4 (2013): A709–A714.

85. J. Z. Lu, B. Han, C. Y. Cui, C. J. Li, and K. Y. Luo, "Electrochemical and Pitting Corrosion Resistance of AISI 4145 Steel Subjected to Massive Laser Shock Peening Treatment With Different Coverage Layers," *Optics & Laser Technology* 88 (2017): 250–262.

86. W. Li, Y. Li, M. Fang, et al., "The Facile in Situ Preparation and Characterization of $C/FeOF/FeF_3$ Nanocomposites as Lib Cathode Materials," *Ionics* 24, no. 6 (2018): 1561–1569.

Supporting Information

Additional supporting information can be found online in the Supporting Information section.